ISSN 1392-1207. MECHANIKA. Vol. 31, No. 3, 2025: 191–198

Experimental Investigation on Fatigue Crack Propagation Under Mixed Mode Loading on Aluminum Alloy AA3033

Hichem MEBARKI*, Hamida FEKIRINI, Mohamed BENGUEDIAB***, Abdelkader LOUSDAD******

**Center of Research in Mechanics (CRM), BP N73B, Freres Ferrad, Ain El Bey, Constantine 25021, Algeria, E-mail: 1993hicham76@gmail.com (Corresponding Author)*

***Laboratory of Mechanics and Physical Materials (LMPM), Faculty of Technology – Department of Mechanical Engineering, University Djillali Liabes of Sidi Bel Abbes, B.P. 89, Cité Ben M'Hidi, Sidi Bel Abbes 22000, Algeria, E-mail: fe_hamida@yahoo.fr*

****Laboratory of Material and Reactive Systems (LMRS), Faculty of Technology -Department of Mechanical Engineering, University Djillali Liabes of Sidi Bel Abbes, B.P 89, Cité Ben M'Hidi, Sidi Bel Abbes 22000, Algeria, E-mail: benguediabm@gmail.com*

*****Laboratory of Mechanics of Structures and Solids (LMSS), Faculty of Technology -Department of Mechanical Engineering, University Djillali Liabes of Sidi Bel Abbes, B.P 89, Cité Ben M'Hidi, Sidi Bel Abbes 22000, Algeria, E-mail: a_lousdad@yahoo.com*

https://doi.org/10.5755/j02.mech.39182

1. Introduction

Designers of metal structures and mechanical systems are constantly faced with fatigue problems. Most fatigue crack propagation tests are carried out under mode I loading conditions. However, these structures in service are often subjected to complex stresses that can generate local loading in mixed modes I, II, and III [1]. This mixed mode of is the most encountered when crack deflection occurs during crack growth [2].

The reliability of metallic structures under repeated loading is evaluated through fracture mechanics, which considers the presence of defects or cracks. This analysis, when combined with experimental or reliability approaches, aids in optimizing design and maintenance to ensure operational safety. To estimate fatigue life and damage under mixed loading, crack propagation kinetics must be understood. Different types of specimens and devices have been designed to carry out tests under different loadings in mixed mode to reproduce the behavior of the material in real service conditions [2-11].Various other techniques are commonly employed for mixed mode I/II fracture testing, such as the use of a Brazilian disc with a central crack [10, 12-14], a rectangular plate containing an inclined central crack subjected to uniform field tension far [15], or even an asymmetrical three- or four-point flexion [16-17].The CTS compression and tension specimen is the most commonly used and can produce a mixed-mode fracture I–III using an adapted loading apparatus and is also used for evaluation of FCG behavior [18-26].The analysis of structural integrity consists of determining the tolerance to damage, taking into account the existence of defects; hence, there is a need to study the behavior of fatigue crack propagation under mixed-mode loading. Experimentation was conducted on specimens (CTS) with different mode I and mode II stress intensity ratios, K_I and K_{II}, in the aluminum alloy AlMgSi1-T6 [27]. Biner [21] carried out tests on AISI-304 stainless steel samples by applying mixed-mode loading (mode I and mode II). In an analysis of the propagation of fatigue cracks in mixed mode (I+II) on steel used in railway structures carried out by Lesiuk et al. [28], the results obtained showed that this approach is essential to guaranteeing the reliability and sustainability of railway infrastructure. Tests were conducted on rail steel class 900A under different loading ratios to study the real fatigue behavior under mixed mode (I + II) [29-30]. A model for predicting the growth path of mixed-mode fatigue cracks in the presence of compressive stresses has been proposed [31]. Others works have been carried out on mixed mode I+II stresses on through cracks, mainly tests on specimens with a central crack or CTS using devices adapted to this type of stress where the mixity of modes is identified by the angle formed between the loading direction and the crack plane [32-34]. Studies highlighted the importance of taking into account the effects of mode mixity and loading rate in predicting the lifespan in mixed mode [35-37]. The prediction of the lifespan is based on the determination of an equivalent stress intensity factor (SIF ΔK_{eq}), taking into account the effects of the two components of the stress [38]. Tanaka modified the Paris model by introducing SIF to determine the life of the component or structure under mixed-mode loading [39].

However, these experimental studies can be costly in terms of time and resources. Therefore, many numerical methods have been developed to predict the mixed-mode propagation fatigue life in a faster and more economical manner [40-42]. These methods involve various criteria such as the maximum circumferential stress (MCS) criterion [43], the maximum energy restitution rate criterion [44], the minimum strain energy density criterion [45], the J integral criterion [46], and the stress intensity factor criterion $K_{II} = 0$ [47]. Additionally, other criteria, like Crack-Tip-Opening-Displacement (CTOD), have been proposed to study the direction and growth rate of cracks under mixed-mode loading. These bifurcation criteria are essential tools for assessing the stability of cracks under static loading and predicting their propagation. For instance, Shanmuga and Murugan's research demonstrated how these parameters influence the tensile behavior of AA2024-T6 joints, offering valuable insights for optimizing the (FSW) process [48]. Additionally, Česnavičius et al work emphasizes the role of numerical modeling in predicting forces and thermal profiles during FSW, further improving the accuracy of weld parameter selection [49].

2. Experimental Investigation

A fatigue crack propagation study under mixed mode (I+II) using CT specimens for three loading angles (45°, 30° and 0°) is presented in this paper. The tests of fatigue crack propagation under mixed mode were conducted in mode I and in mixed mode (I+II) using the CTS specimen and Arcan loading device designed by our laboratory [11] based on the Richards principle [4].

2.1. Experimental procedures

The material studied is a 3003-aluminum alloy type, which is a wrought alloy from the aluminum-manganese family. The material is provided in the form of a sheet measuring 1000x1000x2 mm. The chemical composition and mechanical properties of the material are given in Tables 1 and 2 respectively. The mechanical properties are taken from reference [50].

Table 1
Chemical composition of AA3003 [50]

Elements	Al	Mn	Si	Fe	Cu	Ti	Zn
%	96.7	1.3	0.9	0.9	0,13	0.1	0.03

Table 2
Mechanical properties of base metal AA3003 [50]

Tensile Strength, MPa	Yield Strength, MPa	Poisson's ratio υ	Elastic Modulus E, MPa	Elongation ε, %
156.9	105.7	0.30	70000	15.5

The CTS samples were taken from sheets measuring 360 x 120 mm. The Test samples were obtained from the sheet using water jet cutting process.

The geometry and dimensions of the CTS specimen and the loading device are shown respectively in Fig. 1 and Fig. 2. A pre-crack is introduced at a/w = 0.4 in each specimen (where: a is the length of the crack and w is the width of the specimen). The length of the initial crack is 24 mm. The pre-crack is obtained by water jet cutting up to 20 mm and then machined by milling with a milling cutter in order to obtain the shape of the notch.

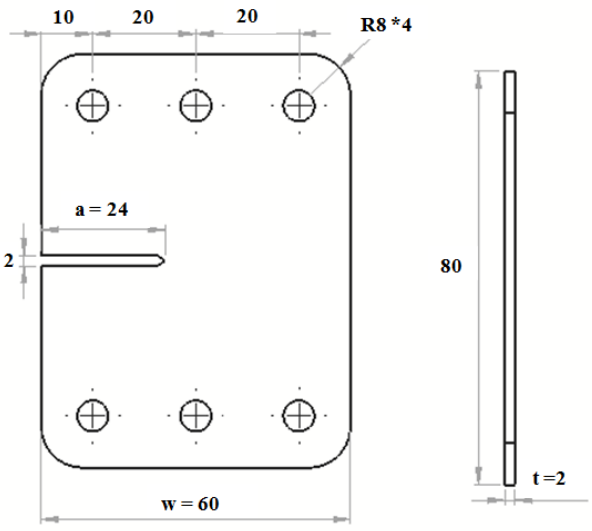

Fig.1 CTS Geometry and dimensions

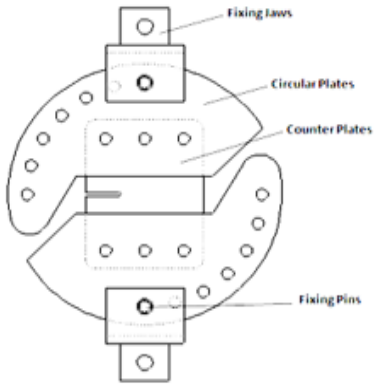

a

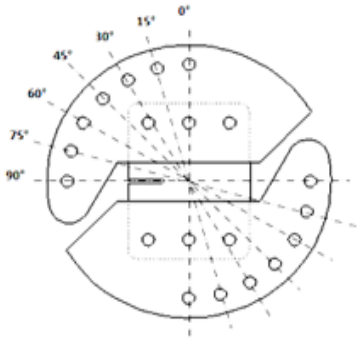

b

Fig. 2 Loading device: a – loading device suitable, b – the different loading modes, [32]

Fig. 3 General view of the bench test and measurement and data acquisition test system

Fatigue tests were carried out on an INSTRON 8501 hydraulic machine with a capacity of 100 kN shown in (Fig. 3). The machine is controlled by a computer equipped with MTS software which allows data acquisition and recording. The fatigue tests were carried out in pure mode I and in mixed mode (I + II) using the CTS(Compact-Tension-Shear) specimen and the specially designed Arcan loading device.

The device allows the application of pure mode(I) loading to pure mode II as well as mixed mode loading on CTS specimens. The loading angle varies in steps of 15° beginning from 0 to 90°. Thus, the loading modes variation

depends on the value of this inclination angle through mode I (pure traction) for an angle of loading 0° and in pure shear mode II for a loading angle of 90°. The geometry and dimensions of the CTS specimen and the loading device are illustrated in Fig. 7. CTS specimens with an initial notch of a = 24 mm. All the specimens were notched by water jet cutting.

The crack length was measured using a magnifying optical binocular telescope (× 40) and a stroboscope mounted on a device attached to the machine (Fig. 4), measuring the length of the crack at x and the height at y (Fig. 5).

We then consider the equivalent length

$$a_{eq} = \sqrt{a^2 + b^2} \ . \qquad (1)$$

Fig. 4 System (Binocular magnifier – Strobe lamp) used for crack tracking

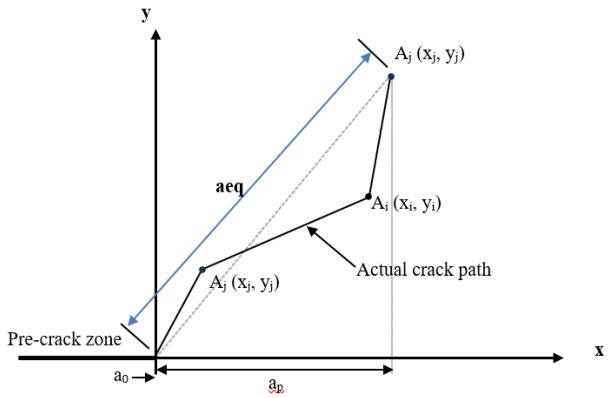

Fig.5 Definitions of extended crack length (a_{eq})

Fig. 6 shows the different configurations of the tests carried out on the CTS (compact tension shear) specimens on the AA3033 aluminum alloy. The choice of the loading angles are 30°, 45° and 0° respectively which correspond to mixed loading (I+II) and pure mode I tension.

The fatigue tests were carried out under mixed loadings with angles of α= 0°, α=30°. and α=45° with a load ratio R = 0.10 and a load (P_{min} = 150 N, P_{max} = 1500 N) and a frequency of 15 Hz.

Fig. 7 shows the different test configurations.

3. Results and discussions

3.1. Crack length-number of cycles curves

The evolution of the equivalent crack length (a_{eq}) as a function of the number of cycles (N) is shown in Fig. 8

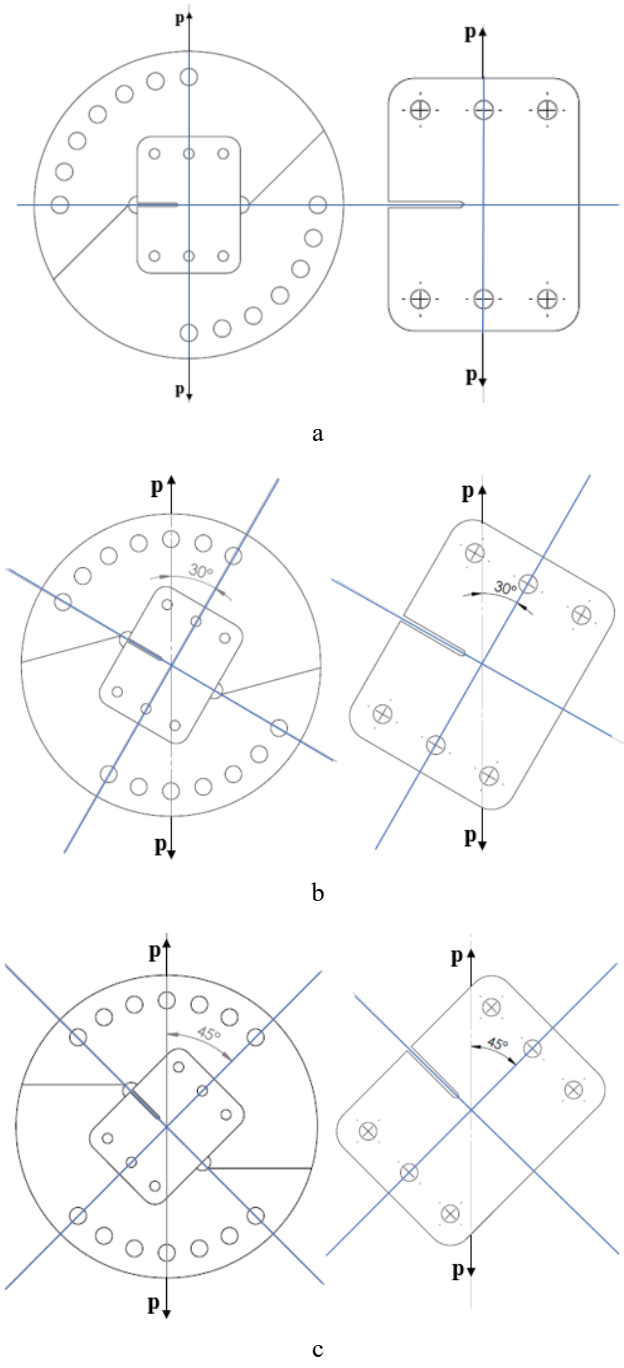

Fig. 6 Specimen mounting on the Loading device suitable for mixed mode: a – α = 0°, b – α = 30°, c – α = 45° [32]

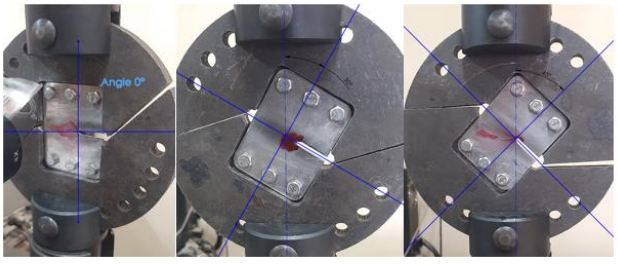

Fig. 7 View of the assembly of the specimens on the device: a – angle α = 0°, b – angle α = 30°, c –angle α = 45°

for the three loading angles (α = 0°, 30°, and 45°). We observe a progressive increase in crack length with the number

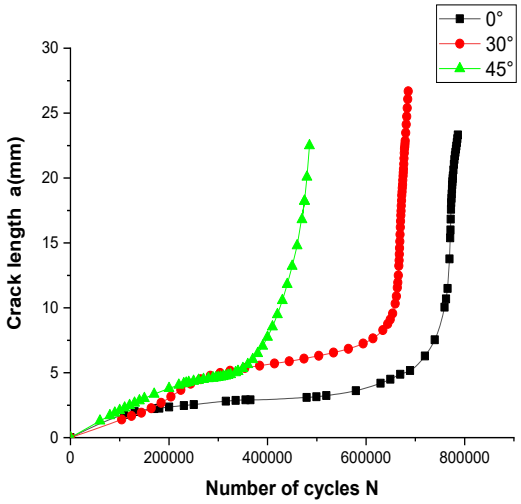

Fig. 8 Crack length with respect to the number of cycles ($\alpha = 0°$, $\alpha = 30°$ and $\alpha = 45°$)

of cycles, which characterizes the phenomenon of fatigue crack propagation. The results show that the crack length increases proportionally to the number of cycles, indicating continuous propagation over time, a phenomenon typical of materials subjected to repeated loading. Analysis of these results provides valuable information on crack propagation under different loading angles. It is also interesting to note that as the loading angle increases, the number of cycles before significant crack propagation increases. Thus, for an angle of 0°, the number of cycles is higher than that observed for 30° and 45°. Additionally, crack propagation is faster at smaller angles due to the increased sensitivity of the structure and the orientation of applied loads, which play a key role in determining the direction of crack propagation. These observations are crucial for assessing the durability and performance of materials under varying loading conditions.

3.2. CTS crack path direction and propagation

Fig. 9 shows the crack propagation direction for loading angle 45° and 30°.

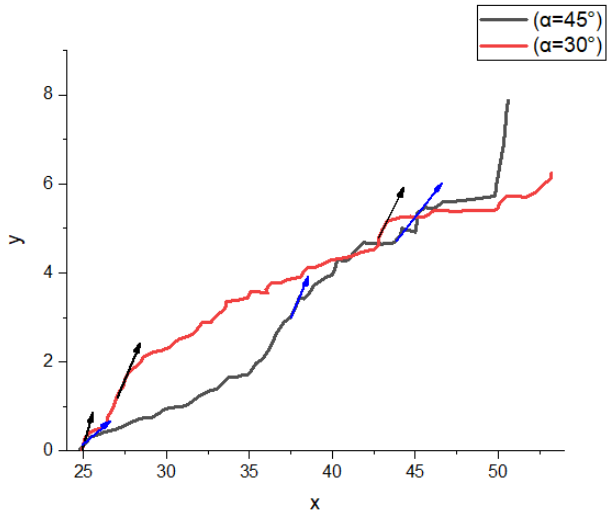

Fig. 9 Direction of propagation of crack in CTS sample for loading angles 45°and 30°

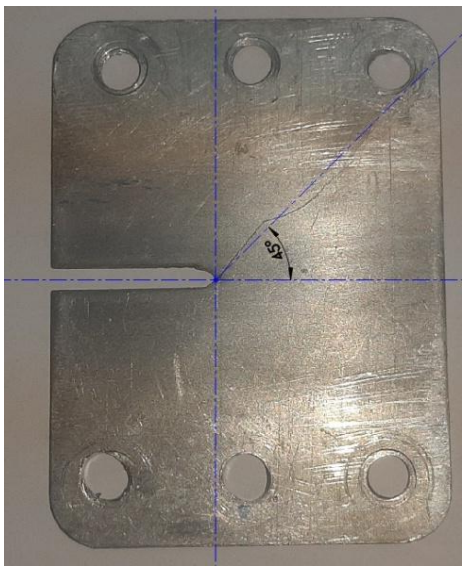

Fig. 10 Example direction of propagation of crack in CTS $\alpha = 45°$

Fig. 9 represent the crack path direction and propagation in the CTS sample for loading angles (α=45°and 30°) several observations can be made:

-The loading angles ($\alpha = 45°$and 30°) are specified which allows understanding how the direction of the load affects the crack propagation. In Fig. 10 the direction of the crack propagation for a loading angle of $\alpha = 45°$ is shown. Different angles can lead to different modes of cracking which is crucial result and information for the design and evaluation of materials structures in terms of fatigue life prediction and reliability.

-By examining the direction of the crack for different loading angles this allows understanding how the applied stresses influence the crack trajectory. This is essential for predicting and preventing structural failures.

-The arrows in the Fig. 9 indicate the direction in which the crack propagates in the CTS sample. This visually depicts and illustrate the crack trajectory under different loading angles.

-Comparing Fig. 9, differences in the direction of crack propagation between 45° and 30° loading angles can be observed. This can provide insights into the structure sensitivity to different loading orientations.

3.3. Crack Propagation growth (*da/dN*) versus the Equivalent Stress Intensity Factor (ΔK_{eq})

The stress intensity factors at the crack tip in mode I and mode II can be calculated using Eqs. (2) and (3) Richard [52]:

$$\Delta K_{\mathrm{I}} = \frac{\Delta P\sqrt{\pi a}}{Wt} cos\,\alpha\, f_{\mathrm{I}}\left(\frac{a}{W}\right), \tag{2}$$

$$\Delta K_{\mathrm{II}} = \frac{\Delta P\sqrt{\pi a}}{Wt} sin\alpha\, f_{\mathrm{II}}\left(\frac{a}{W}\right), \tag{3}$$

where specimen width $W = 60$ mm, the thickness $t = 2$ mm and $\Delta P = 1500$ N.

With $f_{\mathrm{I}}\left(\frac{a}{W}\right)$ and $f_{\mathrm{II}}\left(\frac{a}{W}\right)$ form factors given by

Eqs. (4) and (5)

$$f_{\mathrm{I}}\left(\frac{a}{W}\right)=2.32158-14.3677\left(\frac{a}{W}\right)+66.85752\left(\frac{a}{W}\right)^{2}-117.66921\left(\frac{a}{W}\right)^{3}+89.72502\left(\frac{a}{W}\right)^{4}, \quad (4)$$

$$f_{\mathrm{II}}\left(\frac{a}{W}\right)=-0.05741+4.36076\left(\frac{a}{W}\right)-4.46168\left(\frac{a}{W}\right)^{2}+2.48807\left(\frac{a}{W}\right)^{3}. \quad (5)$$

These equations are valid only in the range of $0.55 < a/W < 0.7$. The variation of the amplitude of the equivalent stress intensity factor in mixed mode

$$\Delta K_{eq}=\sqrt[4]{\Delta K_{\mathrm{I}}^{4}+8\Delta K_{\mathrm{II}}^{4}}. \quad (6)$$

3.4. Comparison crack propagation rate (*da/dN*) versus the equivalent stress intensity factor (ΔK_{eq})

Fig. 11 shows the evolution of the crack propagation rate (*da/dN*) as a function of the variation in the magnitude of the equivalent stress intensity factor (ΔK_{eq}) for three different orientation angles. This figure highlights the differences in crack propagation behavior under different loading directions:

-The evolution of crack propagation rates for the 0° and 30° angles is very similar, indicating comparable propagation characteristics under these loading directions. Furthermore, it is observed that as the crack advances, the crack propagation rate gradually rises, resulting in a corresponding increase in the equivalent stress intensity factor (ΔK_{eq}).

- For the 45° loading angle, crack propagation occurs in two different directions, resulting in a delayed increase in *da/dN*. This behavior suggests a more complex crack propagation process, which may affect the material's fracture performance.

- Overall, the analysis in Fig. 11 provides valuable information on the influence of loading orientation on crack propagation rates, thus facilitating the assessment of material reliability under different stress conditions.

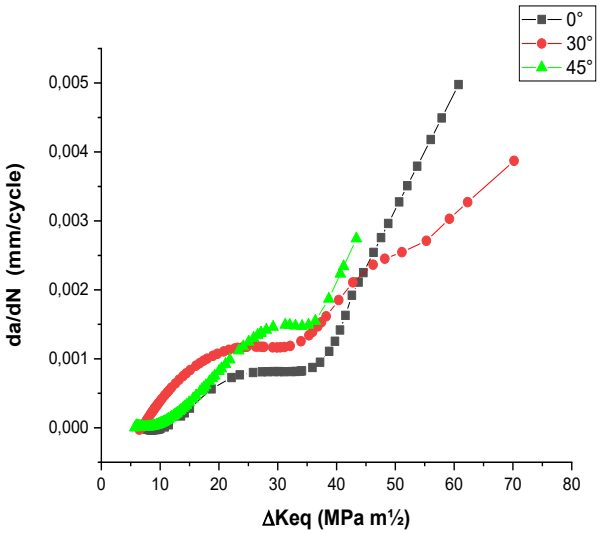

Fig. 11 Crack propagation velocity *da/dN* with respect to the variation in the amplitude of the equivalent stress intensity factor ΔK_{eq} for the three orientation angles

3.5. Evolution of the SIF for mixed-mode FCG

Figs. 12 and 13 present the results of Stress Intensity Factors SIF (Stress Intensity Factor) for Fatigue Crack Growth FCG (Fatigue Crack Growth) in mixed mode I/II at different loading angles where a0 represents the initial crack length (a_0 = 24 mm).

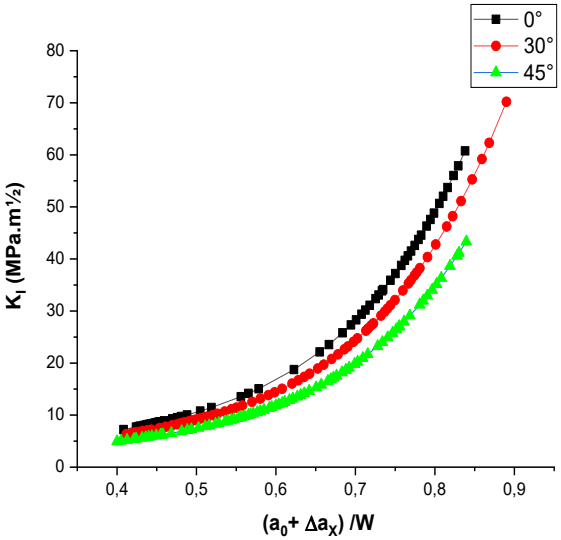

Fig. 12 Evolution of the SIF for mixed-mode FCG K_{I}

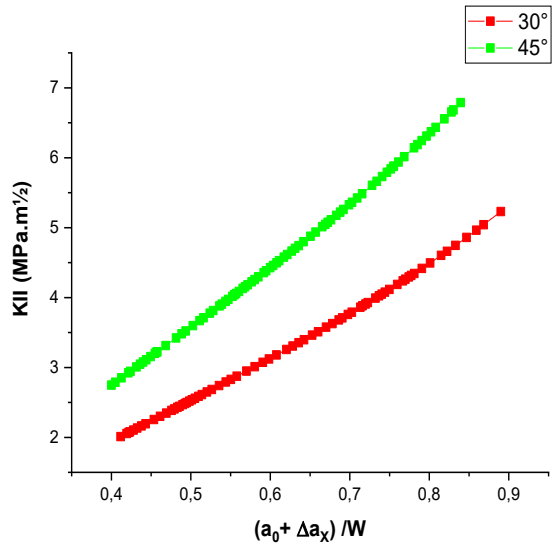

Fig. 13 Evolution of the SIF for mixed-mode FCG K_{II}

Fig. 12 reveals a progressive increase in K_{I} with crack growth leading to an increase in stress concentration at the crack tip. This suggests that the Fatigue Crack Growth Rate (FCGR) increases due to the rising driving force for crack growth. Moreover, the K_{I} curve rises with increasing angle α. It is noticed that K_{I} is the smallest at the 45° angle

while it is largest at 0° angle. This trend is attributed to higher angles resulting in a longer actual crack growth length and a greater driving force for crack growth.

Fig. 13 illustrates the change in K_{II} with crack growth under mixed mode I/II loading. Initially, K_{II} remains positive as long as the crack continues to propagate. The variations in K_{II} at 45° and 30° are not very pronounced which indicate a limited influence on the behavior of FCG at these angles. Thus, the effect of K_{II} on FCG behavior may primarily control the crack growth path but its effect on the FCGR (Fatigue Crack Growth Rate) is not as evident.

Currently, it is recognized that the effect of K_{II} on FCG behavior can not only control the crack growth path but also have a significant influence on the FCGR.

4. Conclusions

In this study, the evolution of crack propagation growth rate for three orientation angles in mixed mode I and II on CTS specimens was experimentally investigated.

The direction of fatigue crack propagation immediately changes relatively to the initial orientation of mode I fatigue when the loading angle is modified. This put into evidence the importance of the loading angle in determining crack propagation behavior.

We observe that the crack propagation for a 30° angle does not have a significant variation compared to the propagation in mode I for α=0°. This finding highlights some resilience of the material at this specific loading angle.

The lifespan for an angle α=45° is significantly shorter compared to those obtained for α=0° and 30°. This difference in lifespan put into evidence the critical importance of the loading angle on the durability of materials subjected to fatigue conditions.

Lastly, these results highlight the significant influence and better understanding of the effect of the loading angle on fatigue crack propagation. The results emphasize the importance of considering this aspect in the design and evaluation of materials subjected to variable loads.

Moreover, the evolution of K_I with crack growth suggests an increase in fatigue crack growth rate. The angle α appears to influence this trend with higher values observed at 0°.

As for K_{II}, its impact on FCG seems primarily related to controlling the crack growth path.

References

1. **Horníková, J.; Šandera, P.; Pokluda, J.** 2004. On the Crack Tip Shielding in Particle Reinforced Composites, Fatigue & Fracture of Engineering Materials and Structures482:311-314. https://doi.org/10.4028/www.scientific.net/MSF.482.311.
2. **Luca, S.; David, T.** 2007.Non-propagating cracks and high cycle fatigue failure in sharply notched specimens under in-phase Mode I and Mode II loading, Engineering Failure Analysis 14(5): 861-876. https://doi.org/10.1016/j.engfailanal.2006.11.038.
3. **Seed, G. M.; Nowell, D.** 1994. Use of the distributed dislocations method to determine the T-stress, Fatigue and Fracture of Engineering Materials and Structures 17: 605-618. https://doi.org/10.1111/j.1460-2695.1994.tb00259.x.
4. **Richard, H. A.; Benitz, K.** 1983. A loading device for the creation of mixed mode in fracture mechanics, International Journal of Fracture 22: R55-R58. https://doi.org/10.1007/BF00942726.
5. **Arcan, M.; Hashin, Z.; Voloshin, A.** 1978. A method to produce uniform plane-stress states with application to fiber-reinforced materials, Experimental Mechanics 18: 141-146. https://doi.org/10.1007/BF02324146.
6. **Marsavina, L.; Linul, E.; Voiconi, T.; Constantinescu, D. M; Apostol, D. A.** 2015. On the crack path under mixed mode loading on PUR foams, Frattura ed Integrita Strutturale (Fracture and Structural Integrity) 9(34): 387-396. https://doi.org/10.3221/IGF-ESIS.34.43.
7. **Williams, J. G.; Ewing P. D.** 1972. Fracture under complex stress – The angled crack problem, International Journal of Fracture Mechanics 8: 441-446. https://doi.org/10.1007/BF00191106.
8. **Ueda, Y.; Ikeda, K.; Kao, T.; Aoki, M.** 1983. Characteristics of brittle fracture under general combined modes including those under bi-axial tensile loads, Engineering Fracture Mechanics 18(6): 1131-1158. https://doi.org/10.1016/0013-7944(83)90007-3.
9. **Awaji, H.; Sato, S.** 1978. Combined Mode Fracture Toughness Measurement by the Disk Test, ASME Journal of Engineering Materials and Technology 100(2): 175-182. https://doi.org/10.1115/1.3443468.
10. **Shetty, D. K.; Rosenfield, A. R.; Duckworth, W. H.** 1987. Mixed-mode fracture in biaxial stress state: Application of the diametral-compression (Brazilian disk) test, Engineering Fracture Mechanics 26(6): 825-840. https://doi.org/10.1016/0013-7944(87)90032-4.
11. **Mebarki, H.; Kebir, T.; Benguediab, M.; Fekirini, H.; Bouchouicha, B.; Lebon, F.** 2022. Experimental and Numerical Study of Fracture Behavior under Mixed-Mode of Al-Alloy AA3003 Not Welded and Welded by FSW Process, Annales de Chimie – Science des Matériaux 46(3): 109-115. https://doi.org/10.18280/acsm.460301.
12. **Seitl, S.; Miarka, P.** 2017 Evaluation of mixed mode I/II fracture toughness of C 50/60 from Brazilian disc test, Fracture and Structural Integrity 11(42): 119-127. https://doi.org/10.3221/IGF-ESIS.42.13.
13. **Levesque, G.; Arakere, N. K.; Mecholsky, J. J.; Gopalakrishnan, K.** 2010. Numerical and experimental investigation of mixed-mode fracture parameters on silicon nitride using the Brazilian disc test, Fatigue and Fracture of Engineering Materials and Structures 33: 490-503. https://doi.org/10.1111/j.1460-2695.2010.01457.x.
14. **Benarbia, D.; Benguediab, M.** 2015. Determination of Stress Intensity Factor in Concrete Material Under Brazilian Disc and Three-Point Bending Tests Using Finite Element Method. Periodica Polytechnica Mechanical Engineering 59(4): 199-203 https://doi.org/10.3311/PPme.8368.
15. **Ueda, Y.; Ikeda, K.; Kao, T.; Aoki, M.** 1983. Characteristics of brittle fracture under general combined modes including those under bi-axial tensile loads, Engineering Fracture Mechanics18(6): 1131-1158. https://doi.org/10.1016/0013-7944(83)90007-3.
16. **Gómez, F. J.; Elices, M.; Berto, F.; Lazzarin, P.** 2007.

Local strain energy to assess the static failure of U-notches in plates under mixed mode loading, International Journal of Fracture 145: 29–45. https://doi.org/10.1007/s10704-007-9104-3.

17. **Marsavina, L.; Constantinescu, D. M.; Linul, E.; Stuparu, F. A.; Apostol, D. A.** 2016. Experimental and numerical crack paths in PUR foams, Engineering Fracture Mechanics167: 68-83. http://dx.doi.org/10.1016/j.engfracmech.2016.03.043.
18. **Aoki, S.; Kishimoto, K.; Yoshida, T.; Sakata, M.; Richard, H. A.** 1990. Elastic-Plastic fracture behaviour of an aluminum alloy under mixed mode loading, Journal of the Mechanics and Physics of Solids 38(2): 195-213. https://doi.org/10.1016/0022-5096(90)90034-2.
19. **Shlyannikov, V. N.** 1999. Mixed-Mode static and fatigue crack growth in central notched and compact tension shear specimens, in Mixed-Mode Crack Behavior ed. Miller, K.; and McDowell, D. ASTM International. https://doi.org/10.1520/STP14254S.
20. **Kim, J. K.; Kim, C. S.** 2002. Fatigue crack growth behaviour of rail steel under mode I and mixed mode loadings, Materials Science and Engineering: A 338(1-2): 191-201. https://doi.org/10.1016/S0921-5093(02)00052-7.
21. **Biner, S. B.** 2001. Fatigue crack growth studies under mixed-mode loading, International Journal of Fatigue 23(1): 259-263. https://doi.org/10.1016/S0142-1123(01)00146-3.
22. **Rozumek, D.; Marciniak, Z.; Lesiuk, G.; Correia, J. A.; de Jesus, A. M. P.** 2018. Experimental and numerical investigation of mixed mode I + II and I + III fatigue crack growth in S355J0 steel, International Journal of Fatigue 113: 160–170. https://doi.org/10.1016/j.ijfatigue.2018.04.005.
23. **Alshoaibi, A. M.** 2022. Crack Growth Analysis under Constant Amplitude Loading Using Finite Element Method, Materials 15(8): 2937. https://doi.org/10.3390/ma15082937.
24. **Demir, O.; Ayhan, A. O.; Iric, S.; Lekesiz, H.** 2018. Evaluation of mixed mode-I/II criteria for fatigue crack propagation using experiments and modeling, Chinese Journal of Aeronautics 31(7): 1525–1534. https://doi.org/10.1016/j.cja.2018.05.009.
25. **Fageehi, Y. A.; Alshoaibi, A. M.** 2020. Numerical Simulation of Mixed-Mode Fatigue Crack Growth for Compact Tension Shear Specimen, Advances in Materials Science and Engineering 2020: 5426831. https://doi.org/10.1155/2020/5426831.
26. **Demir, O.; Ayhan, A. O.; ˙Iriç, S.** 2017. A new specimen for mixed mode-I/II fracture tests: Modeling, experiments and criteria development, Engineering Fracture Mechanics 178: 457–476. https://doi.org/10.1016/j.engfracmech.2017.02.019.
27. **Borrego, L. P.; Antunes, F. V.; Costa, J. M.; Ferreira, J. M.;** 2006. Mixed-mode fatigue crack growth behaviour in aluminium alloy, International Journal of Fatigue 28(5-6): 618-626. https://doi.org/10.1016/j.ijfatigue.2005.07.047.
28. **Lesiuk, G.; Smolnicki, M.; Mech, R.; Zięty, A.; Fragassa, C.** 2020. Analysis of fatigue crack growth under mixed mode (I+II) loading conditions in rail steel using CTS specimen, Engineering Failure Analysis 109: 104354. https://doi.org/10.1016/j.engfailanal.2019.104354.
29. **Nejad, R. M.; Shariati, M.; Farhangdoost, K.** 2019. Prediction of fatigue crack propagation and fractography of rail steel, Theoretical and Applied Fracture Mechanics 101: 320-331. https://doi.org/10.1016/j.tafmec.2019.03.016.
30. **Christodoulou, P. I.; Kermanidis, A. T.; Haidemenopoulos, G. N.** 2016. Fatigue and fracture behavior of pearlitic Grade 900A steel used in railway applications, Theoretical and Applied Fracture Mechanics 83: 51-59. https://doi.org/10.1016/j.tafmec.2015.12.017.
31. **Heirani, H.; Farhangdoost, K.** 2017. Mixed mode I/II fatigue crack growth under tensile or compressive far-field loading, Materials Research Express 4(11): 116505. https://doi.org/10.1088/2053-1591/aa9446.
32. **Otsuka, A.; Tongo, K.; Matsuyama, H.** 1987. Fatigue crack initiation and growth under mixed mode loading in aluminum alloys 2017–T3 and 7075–T6, Engineering Fracture Mechanics 28(5-6): 721-32. https://doi.org/10.1016/0013-7944(87)90065-8.
33. **Lsiuk, G.; Kucharski, P.; Correia, J. A. F. O.; De Jesus, A. M. P.; Rebelo, C.; da Silva, L. S.** 2017. Mixed mode (I+II) fatigue crack growth in puddle iron, Engineering Fracture Mechanics 185: 175-192. https://doi.org/10.1016/j.engfracmech.2017.05.002.
34. **Shlyannikov, V.; Fedotova, D.** 2021. Distinctive features of crack growth rate for assumed pure mode II conditions, International Journal of Fatigue 147: 106163. https://doi.org/10.1016/j.ijfatigue.2021.106163.
35. **Bidadi, J.; Saeidi Googarchin, H.; Akhavan-Safar, A.; da Silva, L. F. M.** 2023. Effects of Mode Mixity and Loading Rate on Fracture Behavior of Cracked Thin-Walled 304L Stainless Steel Sheets with Large Non-Linear Plastic Deformation, Materials 16(24):7690. https://doi.org/10.3390/ma16247690.
36. **Bharadwaj, M. V.; Banerjee, A.** 2014. Effect of Mode-Mixity on Fatigue Crack Growth, Procedia Engineering 86: 653-661. https://doi.org/10.1016/j.proeng.2014.11.066.
37. **Yarullin, R. R.; Yakovlev, M. M.; Boychenko, N. V.; Lyadov, N. M.** 2024. Effect of mixed-mode loading on surface crack propagation in steels, Engineering Fracture Mechanics 295: 109717. https://doi.org/10.1016/j.engfracmech.2023.109717.
38. **Hong, S. H.; Kim, S. D.; Kim, J. H.** 2019. Effects of Mixed Mode Loading Conditions on Fatigue Crack Growth Rate, Key Engineering Materials 814: 176-181. https://doi.org/10.4028/www.scientific.net/KEM.814.176.
39. **Tanaka, K.** 1974. Fatigue crack propagation from a crack inclined to the cyclic tensile axis, Engineering Fracture Mechanics 6(3): 493-498. https://doi.org/10.1016/0013-7944(74)90007-1.
40. **Sander, M.; Richard, H. A.** 2006. Experimental and numerical investigations on the influence of the loading direction on the fatigue crack growth, International Journal of Fatigue 28(5-6): 583-591. https://doi.org/10.1016/j.ijfatigue.2005.05.012.
41. **Wang, H.; Fang, X.; Liu, G.; Xie, Y.; Tian, X.; Leng, L.; Mu, W.** 2021. An Approach to Predicting Fatigue Crack Growth Under Mixed-Mode Loading Based on Improved Gaussian Process, IEEE Access 9: 48777-48792.

https://doi.org/10.1109/ACCESS.2021.3050132.
42. **Qi, S.; Cai, L. X.; Bao, C.; Chen, H.; Shi, K. K.; Wu, H. L.** 2019 Analytical theory for fatigue crack propagation rates of mixed-mode I–II cracks and its application, International Journal of Fatigue 119: 150-159. https://doi.org/10.1016/j.ijfatigue.2018.10.004.
43. **Erdogan, F.; Sih, G. C.** 1963. On the Crack Extension in Plates Under Plane Loading and Transverse Shear, Transaction of the ASME, Journal of Basic Engineering 85(4): 519-525. https://doi.org/10.1115/1.3656897.
44. **Palaniswany, K.; Knauss, W. G.** 1978. On the Problem of Crack Extension in Brittle Solids Under General Loading, Mechanics Today 4: 87-148 https://doi.org/10.1016/B978-0-08-021792-5.50010-0.
45. **Sih, G. C.** 1974. Strain-energy-density factor applied to mixed mode problem, International Journal of Fracture 10: 305-321 https://doi.org/10.1007/BF00035493.
46. **Pawliska, P.; Richard, H. A.; Diekmann, P.** 1993. The behaviour of cracks in elastic-plastic materials under plane normal and shear loading, International Journal of Fracture 62: 43-54 https://doi.org/10.1007/BF00032524.
47. **Cotterell, B.; Rice, J. R.** 1980. Slightly curved or kinked cracks, International Journal of Fracture 16: 155-169. https://doi.org/10.1007/BF00012619.
48. **Shanmuga Sundaram, N.; Murugan, N.** 2009. Dependence of ultimate tensile strength of friction stir welded AA2024-T6 aluminum alloy on friction stir welding process parameters, Mechanika 4(78): 17-24.
49. **Česnavičius, R.; Kilikevičius, S.; Krasauskas, P.; Dundulis, R.; Olišauskas, H.** 2016. Research of the friction stir welding process of aluminium alloys, Mechanika 22(4): 291-296. https://doi.org/10.5755/j01.mech.22.4.16167.
50. **Mebarki, H.; Benguediab, M.; Fekirini, H.; Bouchouicha, B.; Lebon, F.** 2023. Fracture toughness characterization of aluminum allay AA3003 using essential work of fracture concept, Materials physics and mechanics 51(3): 105-114. https://doi.org/10.18149/MPM.5132023_12.
51. **Richard, H. A.** 1985. Fracture predictions for cracks exposed to superimposed normal and shear stresses. Duesseldorf: VDI Verlag. No 631: 60p. Available at: https://inis.iaea.org/records/7xptt-h3237.

H. Mebarki, H. Fekirini, M. Benguediab, A. Lousdad

EXPERIMENTAL INVESTIGATION ON FATIGUE CRACK PROPAGATION UNDER MIXED MODE LOADING ON ALUMINUM ALLOY AA3033

S u m m a r y

The phenomenon of fatigue-crack propagation is a permanent concern for designers, manufactures and users in order to ensure the integrity of structures subjected to cyclical stresses during their operational service. The concept of damage tolerance (DT) is the most commonly used for the design of structures with the prediction of fatigue life crack propagation. Most researchers have focused on studying fatigue crack propagation under mode I loading conditions. However, these structures in service are often subject to complex constraints and combined stresses that can generate local loadings in mixed modes I, II and mode III. In this regard this paper presents a study of fatigue crack propagation in mixed mode (I+II) using CTS (compact-tension-Shear) specimens for three loading angles (45°, 30°, and 0°) respectively. The mixed-mode fatigue crack propagation tests were carried out in modes I and II using the CTS specimen and Arcan loading device specially designed and constructed by our laboratory based on the Richards principle. The experimental results show that the loading angle has a significant effect on the crack growth rate and consequently on the fatigue life prediction of mechanical structure under fatigue loading.

Keywords: CTS specimen, mixed mode fatigue crack growth, Arcan device, fatigue life.

Received October 20, 2024
Accepted June 25, 2025